Controlling solid state gain media by deposition of silver nanoparticles: from thermally-quenched to plasmon-enhanced Nd^{3+} luminescence

Eduardo Yraola,[1] Laura Sánchez-García,[1] Christos Tserkezis,[2] Pablo Molina,[1] Mariola O Ramírez,[1] Jose Luis Plaza,[1] Javier Aizpurua[2] and Luisa E. Bausá[1,*]

[1]*Dpto. Física de Materiales and Instituto Nicolás Cabrera, Universidad Autónoma de Madrid, Madrid, 28049, Spain*
[2]*Center for Materials Physics (CSIC-UPV/EHU) and Donostia International Physics Center (DIPC), Paseo Manuel Lardizabal 4, Donostia-San Sebastián 20018, Spain*
[*]*luisa.bausa@uam.es*

Abstract: We show the possibility of controlling the optical properties of Nd^{3+} laser ions by using different configurations of metallic nanoparticles (NPs) deposited on a solid state gain medium. In particular, we analyze the effect of two different silver NP arrangements on the optical properties of Nd^{3+} ions in $LiNbO_3$: a two-dimensional (2D) high density and disordered Ag NP distribution and a one-dimensional (1D) long single chain of Ag NPs. We demonstrate that while the 2D disordered distribution produces a thermal quenching of the Nd^{3+} luminescence, the 1D single chain leads to the enhancement of the fluorescence from the $^4F_{3/2}$ metastable state. The experimental data are theoretically interpreted by taking into account the different character, radiative or non-radiative, of the localized surface plasmonic modes supported by the Ag nanoparticle distributions at the excitation wavelength. The results point out the capabilities of rare earth ions as optical tools to probe the local plasmonic fields and are relevant to determine the optimal configuration of metallic arrays to improve the performance of potential rare earth ion based sub-micrometer lasers.

OCIS codes: (160.5690) Rare-earth-doped materials; (300.6280) Spectroscopy, fluorescence and luminescence; (160.3380) Laser materials; (250.5403) Plasmonics; (140.3530) Lasers, neodymium.

References and links

1. R. M. Ma, R. F. Oulton, V. J. Sorger, and X. Zhang, "Plasmon lasers: coherent light source at molecular scales," Laser Photon. Rev. **7**(1), 1–21 (2013).
2. O. Hess, J. B. Pendry, S. A. Maier, R. F. Oulton, J. M. Hamm, and K. L. Tsakmakidis, "Active nanoplasmonic metamaterials," Nat. Mater. **11**(7), 573–584 (2012).
3. M. A. Noginov, G. Zhu, A. M. Belgrave, R. Bakker, V. M. Shalaev, E. E. Narimanov, S. Stout, E. Herz, T. Suteewong, and U. Wiesner, "Demonstration of a spaser-based nanolaser," Nature **460**(7259), 1110–1112 (2009).
4. R. F. Oulton, V. J. Sorger, T. Zentgraf, R. M. Ma, C. Gladden, L. Dai, G. Bartal, and X. Zhang, "Plasmon lasers at deep subwavelength scale," Nature **461**(7264), 629–632 (2009).
5. W. Zhou, M. Dridi, J. Y. Suh, C. H. Kim, D. T. Co, M. R. Wasielewski, G. C. Schatz, and T. W. Odom, "Lasing action in strongly coupled plasmonic nanocavity arrays," Nat. Nanotechnol. **8**(7), 506–511 (2013).
6. E. Yraola, P. Molina, J. L. Plaza, M. O. Ramírez, and L. E. Bausá, "Spontaneous emission and nonlinear response enhancement by silver nanoparticles in a Nd^{3+}-doped periodically poled $LiNbO_3$ laser crystal," Adv. Mater. **25**(6), 910–915 (2013).
7. T. Y. Fan, A. Cordova-plaza, M. J. F. Digonnet, R. L. Byer, and H. J. Shaw, "Nd:MgO:$LiNbO_3$ spectroscopy and laser devices," J. Opt. Soc. Am. B **3**(1), 140–148 (1986).
8. S. V. Kalinin, D. A. Bonnell, T. Alvarez, X. J. Lei, Z. H. Hu, R. Shao, and J. H. Ferris, "Ferroelectric lithography of multicomponent nanostructures," Adv. Mater. **16**(910), 795–799 (2004).

#237088 - $15.00 USD Received 27 Mar 2015; revised 24 May 2015; accepted 28 May 2015; published 4 Jun 2015

9. P. Molina, E. Yraola, M. O. Ramírez, J. L. Plaza, C. de las Heras, and L. E. Bausá, "Selective plasmon enhancement of the 1.08 μm Nd^{3+} laser Stark transition by tailoring Ag nanoparticles chains on a PPLN Y-cut," Nano Lett. **13**(10), 4931–4936 (2013).
10. V. Bermudez, M. D. Serrano, and E. Dieguez, "Bulk periodic poled lithium niobate crystals doped with Er and Yb," J. Cryst. Growth **200**(1-2), 185–190 (1999).
11. Y. Sun, B. S. Eller, and R. J. Nemanich, "Photo-induced Ag deposition on periodically poled lithium niobate: Concentration and intensity dependence," J. Appl. Phys. **110**(8), 084303 (2011).
12. Y. Sun and R. J. Nemanich, "Photoinduced Ag deposition on periodically poled lithium niobate: Wavelength and polarization screening dependence," J. Appl. Phys. **109**(10), 104302 (2011).
13. F. J. García de Abajo and J. Aizpurua, "Numerical simulation of electron energy loss near inhomogeneous dielectrics," Phys. Rev. B **56**(24), 15873–15884 (1997).
14. F. J. G. de Abajo and A. Howie, "Retarded field calculation of electron energy loss in inhomogeneous dielectrics," Phys. Rev. B **65**, 17 (2002).
15. S. V. Kalinin and D. A. Bonnell, "Local potential and polarization screening on ferroelectric surfaces," Phys. Rev. B **63**(12), 125411 (2001).
16. H. Loro, M. Voda, F. Jaque, J. G. Sole, and J. E. M. Santiuste, "Polarized absorption of Nd^{3+} in $LiNbO_3$: efect of MgO codoping," J. Appl. Phys. **77**(11), 5929–5935 (1995).
17. A. O. Govorov and H. H. Richardson, "Generating heat with metal nanoparticles," Nano Today **2**(1), 30–38 (2007).
18. D. V. Guzatov, S. V. Vaschenko, V. V. Stankevich, A. Y. Lunevich, Y. F. Glukhov, and S. V. Gaponenko, "Plasmonic enhancement of molecular fluorescence near silver nanoparticles: theory, modeling, and experiment," J. Phys. Chem. C **116**(19), 10723–10733 (2012).
19. K. Lau, I. Staude, Y. Liu, H. Chen, Z. R. Li, and D. N. Neshev, "Ferroelectric domain engineered photochemical deposition for area-selectable broadband enhancement of quantum dot photoluminescence," Adv. Opt. Mater. **1**(10), 720–723 (2013).
20. E. Yraola, L. Sánchez-García, C. Tserkezis, P. Molina, M. O. Ramírez, J. Aizpurua, and L. E. Bausá, "Polarization-selective enhancement of Nd^{3+} photoluminescence assisted by linear chains of silver nanoparticles," J. Lumin., doi:10.1016/j.jlumin.2014.12.053i.
21. R. Esteban, R. W. Taylor, J. J. Baumberg, and J. Aizpurua, "How chain plasmons govern the optical response in strongly interacting self-assembled metallic clusters of nanoparticles," Langmuir **28**(24), 8881–8890 (2012).
22. C. Tserkezis, R. W. Taylor, J. Beitner, R. Esteban, J. J. Baumberg, and J. Aizpurua, "Optical response of metallic nanoparticle heteroaggregates with subnanometric gaps," Part. Part. Syst. Charact. **31**(1), 152–160 (2014).
23. Z. B. Wang, B. S. Luk'yanchuk, W. Guo, S. P. Edwardson, D. J. Whitehead, L. Li, Z. Liu, and K. G. Watkins, "The influences of particle number on hot spots in strongly coupled metal nanoparticles chain," J. Chem. Phys. **128**(9), 094705 (2008).

1. Introduction

A large variety of systems which combine different types of metallic nanostructures, optical emitters, and dielectric media are nowadays the subject of intense activity. In particular, the association of metallic nanostructures with different gain media, has recently given rise to successful configurations such as nanolasers [1,2] from which high energy density can be supplied due to sub-diffraction confinement. Organic dyes and semiconductor based media in association with metallic nanostructures have shown coherent radiation at the nanoscale [3–5]. However, the reports studying the influence of localized surface plasmons (LSPs) on the optical response of trivalent rare earth doped solid state lasers are scarce. Recently, some of the authors have demonstrated the possibility of a remarkable intensification of the spontaneous emission of a Nd^{3+} based solid state laser due to the large local electric fields associated with the LSP from arrays of silver NPs in the proximity of the optically active ions [6]. As a host matrix for the Nd^{3+} active ions, $LiNbO_3$ was chosen, a ferroelectric crystal in which laser action and self-frequency conversion processes have been demonstrated [7].

Due to the polar character of this crystal and taking advantage of the presence of surface charges, metallic silver nanoparticles were photochemically assembled on the $LiNbO_3$ surface by means of ferroelectric lithography [8]. A domain selective deposition was obtained, with the density of the Ag NPs formed on the positive domain surface being much higher than on the negative domain surface. Additionally, a preferential deposition of Ag NPs forming chains on the surface of the antiparallel ferroelectric domain boundaries was also achieved. The LSP resonances supported by those chains of Ag NPs on the ferroelectric domain walls produced an intensification and a strong polarization dependence of the photoluminescence of Nd^{3+} emitting ions in the vicinity of the Ag NPs [6]. This result is of particular interest when the Ag

#237088 - $15.00 USD Received 27 Mar 2015; revised 24 May 2015; accepted 28 May 2015; published 4 Jun 2015

NP chains are distributed parallel to the ferroelectric c-axis of the crystal, on a periodically poled $LiNbO_3$ (PPLN) Y-cut crystal, since the Nd^{3+} laser line at 1.08 μm ($^4F_{3/2}$ $(R_1)\rightarrow$ $^4I_{11/2}(Y_2)$ Stark transition) can be selectively enhanced by exciting with light polarized parallel to the Ag NP chains [9].

Here we compare the effect of two different Ag NP arrangements on the optical properties of Nd^{3+} ions: a 2D high density and disordered Ag NP distribution on positive domain surfaces and a 1D single, long chain of Ag NPs on domain boundaries, both deposited on the relevant Y-cut surface of a Nd^{3+} doped PPLN. While for the 1D distribution an enhancement of the fluorescence is achieved, for the 2D distribution a thermal quenching of the Nd^{3+} luminescence from the $^4F_{3/2}$ metastable state is observed. The results are interpreted taking into account the plasmonic modes supported by finite linear chains of Ag NPs with different number of interacting Ag spheres (from 2 to 15), and considering the 2D configuration as a distribution of short chains randomly oriented, which, as shown later, describes well our experimental NP arrangement. At the visible excitation wavelength used in this work (488 nm) the short-chain plasmonic modes (low number of Ag interacting nanospheres) are characterized by a much larger absorption than that corresponding to a long- chain mode (15 nanoparticles) which, in turn, shows a stronger radiative character. The larger absorption of the 2D Ag NP distribution leads to the presence of heating due to ohmic losses and consequently to the luminescence thermal quenching of Nd^{3+} ion, which could prevent laser action. On the contrary, the lower absorption and the stronger radiative character associated with the 1D distribution of Ag NPs explains the intensification provided by a long single linear chain of Ag NPs. The results show both experimentally and theoretically how by spatially organizing Ag NPs from a 2D disordered configuration to a 1D chain it is possible not only to eliminate the thermal fluorescence quenching, but also to enhance the fluorescence from the Nd^{3+} laser ions. This work is relevant to determine the optimal configuration of metallic arrays to improve the performance of possible rare earth ion based sub-micrometer lasers. Additionally, the results show the potential of optically active ions as tools to investigate the effects of metallic plasmon resonances. In this sense, trivalent rare earth ions provide a great number of crystal field transitions with different character and spectral location suitable to probe the local fields of a variety of metallic configurations.

2. Experimental

Nd^{3+} doped PPLN crystals were grown by the off-centered Czochralski method along the x-axis by adding Nd (1 mol %) in the form of Nd_2O_3. Details on the crystal growth procedure can be found elsewhere [10]. 1 mm thick plates were cut and polished with their main faces oriented parallel to the ferroelectric c-axis (Y-cut).

Photochemical deposition of Ag NPs was achieved by means of ferroelectric lithography following the previously reported procedure [6,11,12]. The crystal surface was illuminated with a UV Mercury pen-lamp (main line at 253.6 nm) while the samples were immersed in a 0,01M $AgNO_3$ at 70 °C. By modifying the time of the process we obtained a 2D high density and random distribution of Ag NPs on positive domain surfaces (20 minutes) or 1D chains of Ag NPs located on the domain wall surfaces (2 min).

Micro-luminescence experiments were carried out with a laser scanning confocal microscope provided with a two-axis XY motorized platform with 0.1μm spatial resolution. An Ar^+ laser at 488 nm was used as excitation source. The laser beam was focused to a spot size less than 1μm, on the surface of the sample and the photoluminescence signal from the samples was collected in backscattering geometry with the same objective. The polarization of the excitation laser beam was parallel to the ferroelectric c-axis of the crystal.

Extinction and absorption spectra were calculated by solving Maxwell's equations with use of the boundary-element method (BEM) [13,14]. Within the BEM, the different inhomogeneous media are described by abrupt interfaces that separate different media characterized by local dielectric functions. The surface charges and currents induced at the

#237088 - $15.00 USD Received 27 Mar 2015; revised 24 May 2015; accepted 28 May 2015; published 4 Jun 2015

interfaces are solved self consistently through a discretization of the boundaries and subsequent solution of the resulting matrix equations. Electromagnetic fields are then calculated in terms of these induced charges and currents. In our systems, full convergence of the results was achieved with use of 2 discretization points per nm at each interface between different materials.

3. Results and discussion

Figure 1(a) shows a SEM image of the selective domain distribution of Ag NPs on the alternating polarity surfaces of a Nd^{3+} doped PPLN-Ycut crystal deposited by the above described photochemical procedure. A 2D high density and disordered distribution of Ag NPs with average size of 50 nm was obtained on the positive polar surfaces. A higher resolution image (see inset) reveals a detail of the Ag NP distribution on the positive domain surfaces as well as the presence of a continuous Ag nanowire on the domain boundary surface. The variation of deposition between domain and boundary has been previously explained considering the polarization screening mechanism and the resultant non-uniform electric field on the crystal surface, which shows a strong component of the electric field in the vicinity of the antiparallel domain boundaries [15]. A very low density distribution of smaller Ag NPs (~20 nm size) on the negative polar surfaces was also observed.

Figure 1(b) shows the unpolarized emission spectra corresponding to the $^4F_{3/2} \rightarrow {}^4I_{11/2}$ transition of Nd^{3+} ions under excitation at 488 nm from the PPLN-Y-cut surface shown in Fig. 1(a). The spectra obtained from the positive domains with high density of Ag NPs and from the negative domains with very low Ag density are plotted in red and blue, respectively. Both spectra display the structure associated with the Stark splitting of the involved $^4F_{3/2}$ and $^4I_{11/2}$ electronic states by the effect of the host crystal field. The number of the observed Stark transitions and their intensity depend on the crystal configuration and polarization, and are in agreement with the non-inversion C_3 local symmetry site of Nd^{3+} ions in $LiNbO_3$ and with the forced electric-dipole character of the Nd^{3+} Stark transitions in this crystal [16]. A comparison between the two emission spectra reveals intensity variations in the relative contribution of some of their bands. Specifically, when the emission spectrum is collected from the surfaces of the 2D high density distribution of Ag NPs, a systematic increase of the high energy bands -shaded region I in Fig. 1(b), accompanied by a decrease of the intensity of the main Nd^{3+} emission line at 1084 nm (region II) is observed. The effect is even more evident when comparing the micro-fluorescence spatial maps from the surface of the Ag deposited PPLN by integrating the Nd^{3+} emission intensity from 1050 to 1070 nm (spectral region I) and by integrating the spectra from 1082 to 1087 nm (spectral region II). These maps are depicted in Figs. 1(c) and 1(d), respectively, and are in agreement with the periodicity observed in the SEM image of the surface. A systematic and periodical increase of the high energy side of the spectrum (region I) arising from areas with a high density of NPs [Fig. 1(c)] is observed. Simultaneously, the map obtained by integrating the intensity of the Nd^{3+} laser transition centred at 1084 nm (region II) results into the negative image, i.e when the density of Ag NPs is high, the main line emission decreases. Furthermore, the total emission area of the $^4F_{3/2} \rightarrow {}^4I_{11/2}$ transition (from 1050 nm to 1120 nm) decreases at the surfaces with high density of Ag NPs, giving rise to a micro-fluorescence map similar to that displayed in Fig. 1(d).

#237088 - $15.00 USD Received 27 Mar 2015; revised 24 May 2015; accepted 28 May 2015; published 4 Jun 2015

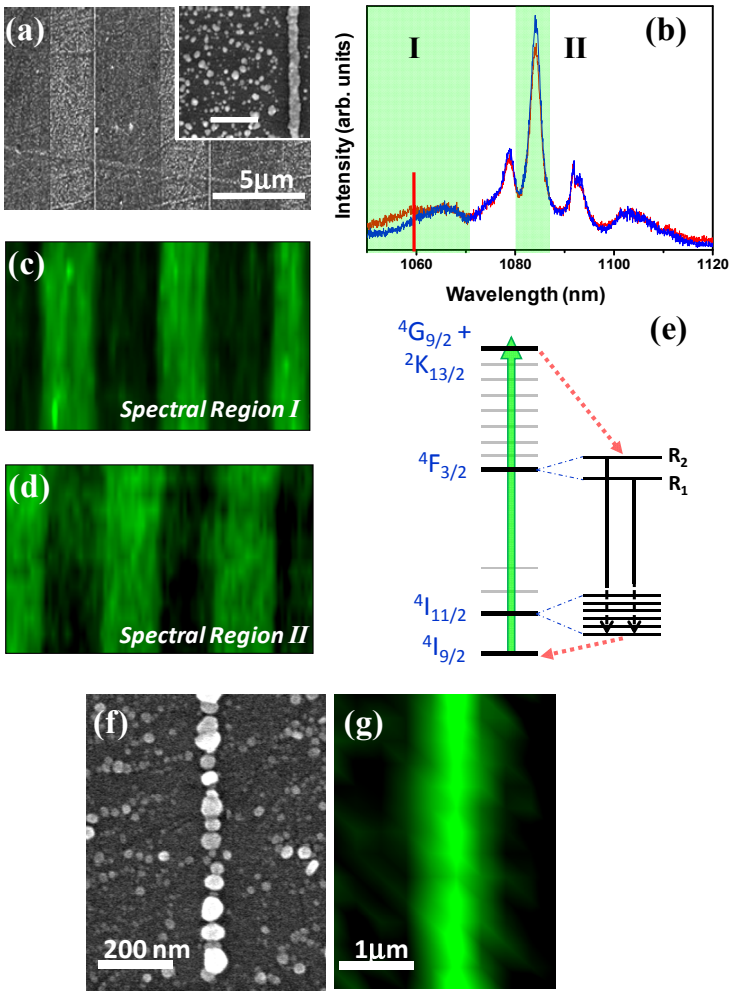

Fig. 1. (a). SEM image of the domain selective distribution of Ag NPs obtained on a Nd^{3+} doped PPLN-Y cut crystal after 20 minutes of UV illumination. A 2D disordered distribution of Ag NPs is preferentially deposited on the positive polar face. (Inset) High resolution image showing a detail of the Ag NP distribution on domain surfaces and the presence of an Ag nanowire parallel to the ferroelectric c-axis of the crystal on a domain wall. The white scale bar corresponds to 500 nm. (b) Unpolarized emission spectra corresponding to the $^4F_{3/2} \rightarrow {}^4I_{11/2}$ laser transition of Nd^{3+} ions collected from regions of low (blue) and high (red) density of Ag NPs. The vertical red line indicates the $^4F_{3/2}$ (R_2) $\rightarrow {}^4I_{11/2}$ (Y_1) thermal transition of Nd^{3+} ions in $LiNbO_3$. (c,d) Micro-fluorescence spatial maps of the integrated Nd^{3+} emission intensity from 1050 to 1070 nm (spectral region I) and from 1082 to 1087 nm (spectral region II), respectively. (e) Schematics of the energy level diagram of Nd^{3+} ions showing the relevant transitions and the crystal field splitting of the $^4F_{3/2}$ and the $^4I_{11/2}$ states. (f) SEM image of one isolated Ag NP chain deposited on the domain wall surface after 2 minutes of UV illumination. (g) Micro-fluorescence spatial map of a single Ag NP chain integrating the $^4F_{3/2} \rightarrow {}^4I_{11/2}$ emission spectrum.

The results can be understood by taking into account that absorption losses of plasmonic nanostructures can efficiently generate heat in the presence of electromagnetic radiation, particularly under the plasmon resonance condition [17]. In fact, the intensity decrease of both the main Nd^{3+} emission line at 1084 nm and the overall $^4F_{3/2} \rightarrow {}^4I_{11/2}$ emission can be attributed to a fluorescence thermal quenching driven by the 2D high density distribution of Ag NPs. This is further supported by the observed increase of the emission at the high energy

#237088 - $15.00 USD Received 27 Mar 2015; revised 24 May 2015; accepted 28 May 2015; published 4 Jun 2015

side of the Nd^{3+} spectrum, which is related to thermal transitions, as explained below. To better illustrate the heating process, Fig. 1(e) shows the Nd^{3+} energy level scheme with the relevant transitions. In $LiNbO_3$, the C_3 crystal field symmetry splits the Nd^{3+} free ion energy states into (2J + 1)/2 Stark crystal field levels. The $^4F_{3/2}$ metastable state splits into two, $^4F_{3/2}(R_1)$ and $^4F_{3/2}(R_2)$, and the $^4I_{11/2}$ state into six ($Y_{1,...,}Y_6$ in order of increasing energy). The relatively small energy gap between the R_1 and R_2 levels (180 cm^{-1} in $LiNbO_3$) [16], makes the $^4F_{3/2}$ (R_2) state especially sensitive to thermal variations so that a moderate increase in temperature produces an increase in the population of the excited Stark component (R_2) of the $^4F_{3/2}$ metastable state and the subsequent intensification of thermal bands. At room temperature most of the transitions from the R_2 level are masked by the dominant emissions coming from the R_1 level with the exception of the $^4F_{3/2}$ (R_2) $\rightarrow ^4I_{11/2}$ (Y_1) which is well isolated at the high energy side of the spectra. The location of this transition is marked on the emission spectra with a vertical red line. Thus, the systematic increase in the intensity of the high energy side of the spectrum (region I) from the high density Ag NP distribution reveals the increase of the thermal population of the $^4F_{3/2}(R_2)$ level. This confirms the presence of heating, which not only modifies the population distribution between the R_1 and R_2 levels, but also produces the activation of non-radiative channels responsible for the observed thermal fluorescence quenching of Nd^{3+} ions. In this respect, it should be taken into account that plasmonic nanostructures could promote fluorescence quenching by processes different than those associated with heating. However, in such a case the spectral shape of Nd^{3+} ions would not be modified. Here, the observed spectral changes in the emission shape of Nd^{3+} ions reflect the thermal origin of the luminescence quenching.

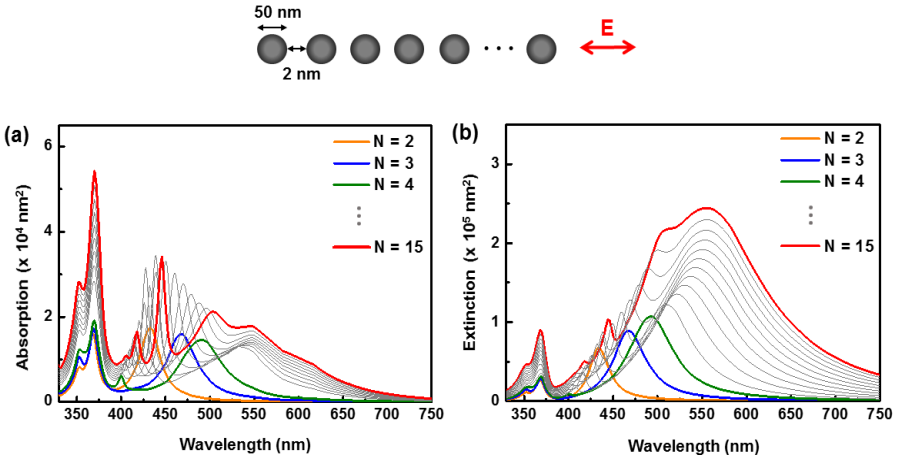

Fig. 2. (a) Absorption and (b) extinction cross section spectra of straight chains of N 50 nm Ag NPs separated by 2 nm gaps calculated for incident light polarized along the chains. Relevant spectra for N = 2, 3 4 and 15 are shown in color. The different order of magnitude between the absorption and the extinction spectra shows the radiative character of the long-wavelength mode for a single long chain of 15 NPs. A scheme of the NP chains and the polarization of the electric field, E, is represented on top.

By modifying the parameters which govern the photochemical deposition a 1D Ag NP arrangement distributed parallel to the ferroelectric c-axis on the domain wall surfaces was obtained [see Fig. 1(f)]. The average size of the NPs forming the chain-like structure is around 50 nm and their separation ranges from 2 to 10 nm. The shape of the Nd^{3+} emission spectrum in the proximity of the chain (obtained under excitation with a beam polarized parallel to the Ag chain) is similar to that shown in Fig. 1(b) (blue). In fact, it coincides with that obtained at room temperature for Nd^{3+} doped $LiNbO_3$ without metallic deposition, and no signs of thermal quenching associated with Ag nanostructures are observed. Moreover, the emitted

#237088 - $15.00 USD Received 27 Mar 2015; revised 24 May 2015; accepted 28 May 2015; published 4 Jun 2015

intensity shows an enhancement in the region of the Ag NP chain. Figure 1(g) shows the corresponding micro-luminescence spatial map illustrating the $^4F_{3/2} \rightarrow {}^4I_{11/2}$ integrated emission spectra in the proximity of the long chain of NPs where an intensification of around 30% is observed [9], in agreement with previous results in fluorophore/Ag NP combinations [18]. These results point out the key role of the Ag NP assembly on the hybrid metal-ferroelectric heterostructures to control the optical properties of laser ions. While the 2D disordered distribution of Ag NPs produces a thermal quenching of the Nd^{3+} spontaneous emission, the 1D distribution of Ag NPs in isolated and long chains supports the enhancement of the fluorescence. Additionally, an area-selectable enhancement of luminescence is also possible as reported for our system as well as for other emitters [6, 19].

To get further insight into the role of the different Ag NP configurations on the spectroscopic properties of Nd^{3+} ions we have analyzed the spectral differences of plasmonic modes associated with silver nanospheres distributed both in short and long linear chains. For that purpose the absorption and extinction cross section spectra of chains formed by different number, N, of Ag NPs have been calculated. Figures 2(a) and 2(b) show the results for N ranging from 2 up to 15. In all cases, the calculations were performed considering spherical Ag NPs with an average size of 50 nm and interspacing distances of 2 nm forming a perfectly straight chain. The polarization of the incident plane wave was chosen parallel to the chain. Here it is important to mention that mixing spheres of different sizes leads to modes at intermediate wavelengths, so that the final result is equivalent to studying a chain of spheres with a size corresponding to the average size of the distribution. Therefore, the deposited metallic structures can be well modeled by chains of spheres with a size corresponding to that average size, 50 nm in our case. The specific distribution size as well as the effect of the particle size, and the effect of mixing NPs with different sizes on the extinction cross section spectra of chains of Ag NPs on $LiNbO_3$ can be found elsewhere [20].

On the other hand, as shown in previous works, the spectra for moderately disordered chains remain remarkably close to the results of the perfectly straight chains [21, 22]. For illustrative purposes the spectra associated with N = 2, 3, 4 and 15 nanoparticles are plotted with different colors in Fig. 2. The absorption spectra in Fig. 2(a) can be divided into two different spectral ranges: the high (λ = 325 - 400 nm) and the low energy region (λ > 400 nm). The high energy region is governed by the contribution of the single plasmon resonance of 50 nm Ag NPs, and increases with N while maintaining both the spectral shape and the energy position. The low energy region accounts for the coupling between the Ag NPs forming the chains and depends strongly on the number of interacting NPs [21]. Moreover, as N increases there is a red shift accompanied by a broadening of the absorption bands due to the presence of higher order collective interactions supported by the chains. Additionally, there is also a significant dependence of sharp resonances (absorption bands), associated with higher-order modes, within the 400-500 nm spectral range. This spectral region is of particular interest in the context of our work since it contains the excitation wavelength (λ = 488 nm) used for the photoluminescence experiments.

The extinction cross section spectra are shown in Fig. 2(b). Similarly to the absorption, the intensity of the single plasmon resonances at 370 nm increases with N. Additionally, the dimers and short-chain modes (N = 2, 3 and 4) display broad resonances centered at 432 nm, 467 and 493 nm, respectively. For larger N values, the main mode broadens and shifts to longer wavelengths. A convergence of the position of the main mode at around 580 nm is obtained for chains of about 15 NPs. Indeed, increasing the number of interacting NPs above N~10 does not substantially change the spectral shape of the extinction spectrum, but only its intensity. It is important to note that the extinction values for the long-wavelength mode are one order of magnitude larger the values obtained for the absorption at similar wavelengths pointing out the strong radiative nature of the long-chain mode compared to those of single Ag NPs or short chains, in agreement with previous works predicting the influences of particle number in strongly coupled metal NP chains [23]. Once the plasmonic modes

#237088 - $15.00 USD Received 27 Mar 2015; revised 24 May 2015; accepted 28 May 2015; published 4 Jun 2015

supported by linear chains of N Ag NPs have been analyzed, the plasmon enhanced Nd^{3+} emission related to the 1D long single chain [Fig. 1(g)], and the Nd^{3+} luminescence thermal quenching associated with the 2D distribution of Ag NPs [Fig. 1(d)] can be explained. In this latter case the 2D disordered configuration of Ag NPs [Fig. 3(a)] can be interpreted as a distribution of short linear chains randomly oriented [Fig. 3(b)], and can be compared to the 1D system illustrated in Fig. 3(c).

Figure 3(d) shows a SEM image with a detail of the 2D distribution of Ag NPs formed on the domain surfaces. For illustrative purposes, some short chains have been marked with colored boxes. The SEM image of the long chain of Ag NPs formed on the domain boundary surfaces is shown in Fig. 3(e).

By using different high resolution SEM images we first performed a statistical analysis in 5x5 μm^2 spatial regions to determine: i) the average size of the NPs, which was found to be close to 50 nm, ii) the percentage of short chains among the total distribution that was composed by dimers (36%) and short N-chains with N = 3 (37%) and N = 4 (22%), and iii) their orientation with respect to the axis of polarization of the incoming light, which strongly governs the optical response of a given linear chain. The distribution of short chains was used to estimate an effective average absorption coefficient $\alpha_{eff}(\lambda)$ by:

$$\alpha_{eff}(\lambda) = \sum_{N} \frac{1}{A_N} \chi_N \cos\theta_N Abs_N(\lambda) \quad (1)$$

where N is the number of NPs in a considered N-chain, A_N its area calculated as N times the area of a single NP, χ_N is the fraction of the N-chain contributing to the optical response, $<\cos\theta_N>$ accounts for the orientation of the chains (projecting the absorption on the direction of the polarization of the excitation beam) and $Abs_N(\lambda)$ the theoretically calculated absorption cross-section spectrum of a single N-chain from Fig. 2(a). For the sake of comparison, for the 1D distribution (formed by 15 NPs), the cross section obtained from the calculations was divided by its area, considered as 15 times the area of a single sphere. The results of the effective absorption coefficient corresponding to each configuration are shown in Fig. 3(f). As observed, for the excitation wavelength used in our experiments (488 nm) the effective absorption of the disordered 2D configuration is around twice the absorption obtained for the single long chain. This results into a considerable heating effect (absorption losses) in the proximity of the NPs, hence limiting the final operation of the 2D hybrid metal-ferroelectric heterostructure. These results are consistent with scanning confocal photoluminescence experiments which show a thermal quenching of the luminescence from the $^4F_{3/2}$ metastable state at the spatial regions with high density 2D distribution of Ag NPs. On the contrary, the lower absorption and the stronger radiative character associated with the 1D single chain explains the intensification provided by the long linear chains of Ag NPs.

#237088 - $15.00 USD Received 27 Mar 2015; revised 24 May 2015; accepted 28 May 2015; published 4 Jun 2015

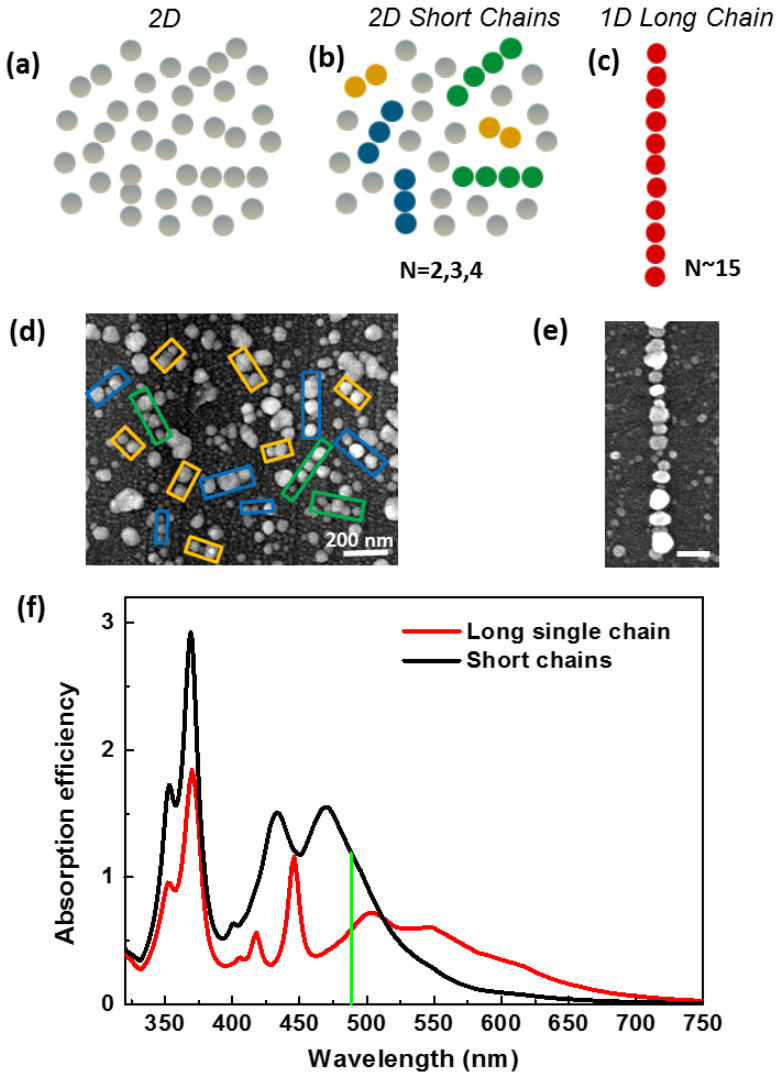

Fig. 3. (a-c) Schematics of the analyzed Ag NP arrangements. As illustrated in panel (b) the 2D disordered distribution of Ag NPs can be interpreted as a distribution of short linear chains randomly oriented (colored in yellow, blue and green for N = 2, 3 and 4, respectively. (d) SEM image of 2D disordered distribution of Ag NPs. Silver NPs are grouped as short chains with colored boxes. (e) SEM image of a single 1D long chain. White bar corresponds to a 100nm length. (f) Effective average absorption calculated for the 2D disordered Ag Np distribution (black spectrum) and for the long single chain (red spectrum). The incident wavelength (488 nm, coinciding with the $^4I_{9/2} \rightarrow {}^4G_{9/2} + {}^2K_{13/2}$ transition of Nd^{3+} ions) is marked by a green vertical line.

4. Summary

In conclusion, the possibility of controlling the properties of optically active rare earth ions by different arrays of metallic nanoparticles is demonstrated. By organizing silver NPs from a 2D disordered configuration to a 1D single chain it is possible not only to eliminate the thermal fluorescence quenching, a crucial feature that could prevent laser action, but also to enhance the fluorescence from the Nd^{3+} laser ions. The results are relevant to determine the optimal configuration of arrays of silver NPs which improve the performance of solid state gain media

#237088 - $15.00 USD Received 27 Mar 2015; revised 24 May 2015; accepted 28 May 2015; published 4 Jun 2015

and constitute a necessary step to study the interaction between metal nanostructures and optically-active ions, which is of interest in the field of solid state based sub-micrometric lasers or gain-enhanced metamaterials.

Acknowledgments

This work has been supported by the Spanish Ministry of Economy and Competitiveness (MINECO) under projects MAT2010-17443 and MAT2013-43301-R and Comunidad de Madrid under grant S2013/MIT-2740. CT and JA acknowledge financial support from Project FIS2013-41184-P of the Spanish MINECO, project ETORTEK NANOGUNE'14 of the Department of Industry of the Basque Government, and from the Department of Education of the Basque Government, IT756-13 of consolidated groups. MOR acknowledges Ramon y Cajal Contract from Spanish MINECO. LSG acknowledges FPU13/02476 grant from the Spanish Ministry of Education.

#237088 - $15.00 USD Received 27 Mar 2015; revised 24 May 2015; accepted 28 May 2015; published 4 Jun 2015